J Math Chem (2015) 53:41–57
DOI 10.1007/s10910-014-0409-y

ORIGINAL PAPER

Some remarks on the model of the extended gentlest ascent dynamics

Josep Maria Bofill · Wolfgang Quapp · Efrem Bernuz

Received: 16 July 2014 / Accepted: 13 September 2014 / Published online: 30 September 2014

Abstract The study of molecular systems involves models describing the evolution of the system through barriers separating basins of attraction on a high dimensional potential energy surface. It is a challenge problem inherent to a complex molecular system. Recently Samanta and E (J Chem Phys 136:124104, 2012) have proposed an extended gentlest ascent dynamics where the system should hop from one saddle point on a potential energy surface to a next saddle point. In the present study we do an analysis of this dynamical model using different two-dimensional potential energy surfaces. The extended gentlest ascent dynamics is a model that corresponds in its mathematical formulation to a set of first order ordinary differential equations. Due to this fact the initial conditions and features are also studied to see their effect on the dynamical behavior.

Keywords Potential energy surface · Extended gentlest ascent · Saddle point hopping · Test examples

J. M. Bofill (✉) · E. Bernuz
Departament de Química Orgànica, Universitat de Barcelona,
Martí i Franquès 1, 08028 Barcelona, Spain
e-mail: jmbofill@ub.edu

J. M. Bofill
Institut de Química Teòrica i Computacional, Universitat de Barcelona (IQTCUB),
Martí i Franquès, 1, 08028 Barcelona, Spain

W. Quapp (✉)
Mathematisches Institut, Universität Leipzig, PF 100920, 04009 Leipzig, Germany
e-mail: quapp@uni-leipzig.de

1 Introduction

One of the main problems in theoretical chemistry is the study of the mechanisms associated with chemical reactions. An important achievement in the development of models to understand the chemical reaction mechanisms was the introduction of the following two concepts, namely, the potential energy surface (PES) and the reaction path (RP) as a way to describe the molecular system evolution from reactants to products in geometrical terms [1,2]. The impact of these concepts in chemistry during the last half century can be justified by the intuitive and easy manner to visualize the evolution of any chemical reaction and its qualitative prediction power. The fact was motivated by a continuous mathematical development on the grounds of the model and computational algorithms to compute an RP as well. The basic definition of an RP is a curve located in the configuration space of the molecule. Its energy profile monotonically increases from a minimum to a first index saddle point and from that point it monotonically decreases to a new stationary point, usually again a minimum. If $\mathbf{q}$ is a coordinate vector of dimension N, then the RP is represented by $\mathbf{q}(t)$, being t the parameter that characterizes the curve called reaction coordinate. Normally, the parameter, t, is the arc-length of the curve.

The RPs are static curves on the PES, which means that only geometric properties of the PES are taken into account and no dynamical information can be sought from these pathways. An effort to incorporate a dynamical information while, at the same time, keeping the philosophy of envisaging the reaction as a single path on the PES, was introduced with the formulation of the reaction-path Hamiltonian (RPH) [3]. It views the reaction as a vibrating molecule, for which some geometric parameters undergo dramatic changes; the parameter, t, most properly describes the reaction and it is very often taken as the reaction coordinate, whereas the remaining degrees of freedom experience some changes in the nature of the associated vibrational motion. Classical and quantum RPHs have been proposed recently [4–6]. Reaction theories like the famous transition state theory and the variational transition state theory are also based at least implicitly or explicitly on the RP model [7]. Nevertheless, many times a well selected RP curve very closely matches the average line of a set of molecular dynamical trajectories [8]. Perhaps the observation gives physical grounds to the RP model.

Nowadays, chemists and theoreticians are interested in the description of complex molecular systems. In contrast to simple molecules, the dynamics of complex systems evolve, in a more frequent way, via a sequence of rare and infrequent intermediates or metastable states [9]. In the dynamical evolution the appearance of different time scales characterizes the metastability. In a very simplified way, there are two time scales, namely, the relaxation time scale of a state and the transition time scale out of a state. We say that a state is metastable if the second time is larger than the first. From the above classification one concludes that transitions between metastable states are rare or infrequent events. If the molecule is a non-complex system, the associated PES is simpler, and we assume that the molecule moves along the RP, the bottleneck for the transient evolution is a stationary point of index one, also called transition state (TS), of the PES. The RPs are important in low temperature dynamics of the molecular system. At higher temperatures, the RP can still correspond to the path of maximal

probability of the dynamical evolution and hence a knowledge of the stationary point of index one becomes important [8].

There exist many curves on the PES that satisfy the RP conditions. The fact is the reason of the variety of RP curves. In particular, curves are interesting that climb out of basins of attraction. The curve most widely used as an RP is the so-called intrinsic reaction coordinate (IRC); the curve is the steepest descent of a TS in mass weighted coordinates [10]. It joins two minima through one TS [11]. Another curve used as an RP is the distinguished or driven coordinate method [12–14], or the more recent version, the so-called reduced gradient following (RGF) [15,16], also labeled as Newton path or Newton trajectory (NT) [17,18]. Additionally, we have the gradient extremals (GEs) [19–24]; however, their computational demand limits their applicability [25]. A mathematical ground of all previous RP curves is the theory of Calculus of Variations. This type of RP curves is of variational nature [18,24,26–28]. It implies that theoretically some well defined ordinary differential equations are derived being associated to the curve that extremalizes a corresponding functional of the variational problem. The integration of the associated ordinary differential equations results in the desired type of an RP.

There is a further long list of algorithms to climb out of the basins of attraction of a minimum on the PES. The algorithms describe paths that in principle reach the first index saddle point, and in contrast to that mentioned previously, some of them are not related to an established ordinary differential equation. The first one is due to Crippen and Scheraga [29]. In the algorithm, at an iteration, lets say k, the next point is obtained by the minimization of the PES on a hyperplane with a given normal vector, $\mathbf{r}$. The method can be seen as a special case of the distinguished coordinate method [18]. A great number of the algorithms is based on a generalization of the Levenberg-Marquardt method [30] that basically consists of a modification of the Hessian matrix to achieve both, first the correct, desired spectrum of the Hessian at the stationary point, and second to control the length of the displacement during the location process. There is a large set of methods that fall into this class [31–39]. An algorithm that evaluates a steepest descent/ascent curve direction avoiding the construction of the full Hessian is the dimer method proposed by Henkelman and Jónsson [40]. The idea has been improved and generalized several times, see e.g. ref. [41]. The active relaxation technique (ART) proposed by Barkema and Mousseau [42] is another algorithm to explore the PES. However, the curve described by the ART method may not pass through the first index saddle point.

More recently, the gentlest ascent dynamics (GAD) has been proposed [43]. The basic idea of the algorithm is to formulate an evolution of the curve such that it is convergent at a first index saddle point. The convergence to this type of stationary points is guaranteed theoretically [43], if the method converges, at all. The GAD algorithm can be seen as an improvement of the Smith [44,45] method proposed some time ago. Recently the GAD technique has been analyzed by Bofill and Quapp [46,47] concluding that the general behavior of this algorithm is that it can directly find the transition state of interest by a gentlest ascent, or it can go a roundabout way over a turning point (TP) and then find the transition state going downhill along a ridge. A technique based on the Krylov space to solve GAD equations has been proposed recently [48]. Finally, Samanta and E [49] have been extended the GAD algorithm to

a tool for sampling saddle points and for a successive exploration of the configuration space of the PES. This tool is a dynamical version of the GAD algorithm, called MD-GAD, which describes trajectories that can hop from one saddle point region to another saddle point region.

In this article we analyze the MD-GAD algorithm for some non-periodic two-dimensional PESs with different initial conditions. The reported PESs represent general surfaces associated to a mechanism of a generic chemical reaction. This paper is organized as follows: in Sect. 2 the basis of the GAD model is briefly reviewed and some features of this type of curves are discussed as well. The extended GAD model of Samanta and E [49] is introduced. We argue this extended model using the Theory of Calculus of Variations [50]. The nature of the turning points of this dynamical model is also reported. In Sect. 3 we show in a set of two-dimensional PESs the behavior and features of the trajectories of the MD-GAD model. Finally, some conclusions are drawn.

2 The basic equation

Let us denote by $W(\mathbf{q})$ the PES function and by $\mathbf{q}^T = (q_1, \ldots, q_N)$ the coordinates. The dimension of the $\mathbf{q}$ vector is N, the number of the degrees of freedom of interest. The superscript T means vector- or matrix transposition. We assume that the PES function admits a local gradient vector, $\mathbf{g}(\mathbf{q}) = \nabla_{\mathbf{q}} W(\mathbf{q})$, and a Hessian matrix, $\mathbf{H}(\mathbf{q}) = \nabla_{\mathbf{q}} \nabla_{\mathbf{q}}^T W(\mathbf{q})$ at every interesting point, $\mathbf{q}$. Now, let us consider the family of (abstract) image functions of $W(\mathbf{q})$, labeled by $\Theta(\mathbf{q})$, where the gradient vector of this image functions is defined by

$$\nabla_{\mathbf{q}} \Theta(\mathbf{q}) \ := \mathbf{f}(\mathbf{q}) = \mathbf{U}_{\mathbf{v}} \mathbf{g}(\mathbf{q}) = \left[\mathbf{I} - 2 \frac{\mathbf{v}(\mathbf{q}) \mathbf{v}^T(\mathbf{q})}{\mathbf{v}^T(\mathbf{q}) \mathbf{v}(\mathbf{q})} \right] \mathbf{g}(\mathbf{q}) \tag{1}$$

where $\mathbf{f}(\mathbf{q})$ is named the image gradient vector, $\mathbf{U}_{\mathbf{v}}$ is the Householder orthogonal matrix constructed by an arbitrary guide vector, $\mathbf{v}(\mathbf{q})$, being in principle a function of $\mathbf{q}$, and $\mathbf{I}$ is the unit matrix. $\mathbf{f}(\mathbf{q})$ is explicitely determined by $\mathbf{v}$ and $\mathbf{g}$, however, $\Theta(\mathbf{q})$ itself is unknown. If one assumes two special cases, we find the following action of $\mathbf{U}_{\mathbf{v}}$:

(i) if $\mathbf{v}$ is orthogonal to $\mathbf{g}$ then $\mathbf{U}_{\mathbf{v}}$ is the identity operator, $\mathbf{U}_{\mathbf{v}}\ \mathbf{g} = \mathbf{g}$, and $\mathbf{f}(\mathbf{q})$ is the steepest ascent on the PES, W; however,
(ii) if $\mathbf{v}$ is parallel to $\mathbf{g}$ then it is $\mathbf{U}_{\mathbf{v}}\ \mathbf{g} = -\mathbf{g}$, and $\mathbf{f}(\mathbf{q})$ is the steepest descent.

Thus, by the choice of $\mathbf{v}$ we can put all directions between $\mathbf{g}$ and $-\mathbf{g}$ for $\mathbf{f}(\mathbf{q})$ in the plane spanned by $\mathbf{v}$ and $\mathbf{g}$. Now we can take the image gradient field of the (abstract) image function, given in Eq. (1), to define a field of curves as

$$\frac{d\mathbf{q}}{dt} = -\mathbf{f}(\mathbf{q}) = -\mathbf{U}_{\mathbf{v}} \mathbf{g}(\mathbf{q}) = -\left[\mathbf{I} - 2 \frac{\mathbf{v}(\mathbf{q}) \mathbf{v}^T(\mathbf{q})}{\mathbf{v}^T(\mathbf{q}) \mathbf{v}(\mathbf{q})} \right] \mathbf{g}(\mathbf{q}) \tag{2}$$

where t is the parameter that characterizes the curve, $\mathbf{q}(t)$. The usual case for a TS search is the following: if the curve $\mathbf{q}(t)$ is in the TS col, and if $\mathbf{v}(t)$ points along

this valley, then the energy is ascending along the **v**-vector direction on the actual PES whereas it is descending along the set of $(N-1)$ linear independent directions orthogonal to the **v**-vector. Equation (2) is the first equation that governs the GAD model [43] but it is also used by the ART [42] as well as by the string [51] methods to locate first index saddle points. The above reasoning is based on Smiths's theory of an image function [44], however some criticism and limitations to the theory have been pointed out elsewhere [45,46]. By Eq. (2) the gradient is mirrored at a fixed direction **v**. This is not flexible enough. To complete the model, an equation for a development of the **v**-vector should be given additionally. In the ART method the **v**-vector is constructed by the normalization of the $\mathbf{q}-\mathbf{q}_0$ vector, whereas in the string method it is the normalized tangent vector of the current curve. In the GAD method the equation that governs the **v**-vector is

$$\frac{d\mathbf{v}}{dt} = -\left[\mathbf{I} - \frac{\mathbf{v}(\mathbf{q})\mathbf{v}^T(\mathbf{q})}{\mathbf{v}^T(\mathbf{q})\mathbf{v}(\mathbf{q})}\right]\mathbf{H}(\mathbf{q})\mathbf{v}(\mathbf{q}) \tag{3}$$

which is a rule for a descent direction along $\mathbf{v}(\mathbf{q})$ multiplied with the Hessian matrix, **H**, minus the Raiyleigh–Ritz function, $\lambda_{\mathbf{q}}(\mathbf{v}) = \mathbf{v}^T\mathbf{H}(\mathbf{q})\mathbf{v}/\mathbf{v}^T\mathbf{v}$. Thus

$$\frac{d\mathbf{v}}{dt} = -\left[\ \mathbf{H} - \lambda_{\mathbf{q}}\,\mathbf{I}\right)\ ]\,\mathbf{v}.$$

If **v** is an eigenvector of **H** then Eq. (3) does not change anything. However, if **H** changes itself with **q**, together with its eigenvectors, then a change of the vector **v** can happen that acts back to Eq. (2). If **q** is near a TS, and if **v** is an eigenvector of **H** then Eq. (3) is zero and from Eq. (2) follows $d\mathbf{q}/dt$ goes to zero with the disappearance of the gradient. At the TS the system of Eqs. (2) and (3) converges [43]. The dimension of the system is $2N$.

Another effect of the GAD trajectories is that there can emerge turning points (TP) [46]. At a TP the tangent to the GAD curve has to point orthogonally to the gradient. The vector $d\mathbf{q}/dt = -\mathbf{U}_{\mathbf{v}}\mathbf{g}$ has to lie in the tangential hyperplane of the equipotential hypersurface of the PES. This happens if the mirror line (or plane) being orthogonal to **v**, and belonging to the Householder matrix, $\mathbf{U}_{\mathbf{v}}$, has an angle of $\pi/4$ to the gradient. There **g** and **v** cannot be eigenvectors at the same time, see Scheme 1.

Scheme 1 Gradient vector and guide vector **v** at a TP of a GAD trajectory. Here is $\mathbf{g} \perp -\mathbf{U}_{\mathbf{v}}\mathbf{g}$

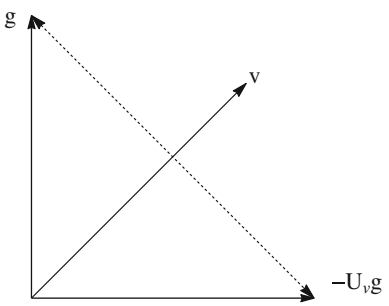

Equations (2) and (3) define the tangent of the GAD curve. If one is interested to locate a stationary point of an index higher than one, say s, the GAD method can be generalized adequately. In this case Eqs. (2) and (3) take the form,

$$\frac{d\mathbf{q}}{dt} = -\,[\,\mathbf{I} - 2\mathbf{V}(\mathbf{q})\mathbf{V}^T(\mathbf{q})\,]\,\mathbf{g}(\mathbf{q}) \tag{4}$$

$$\frac{d\mathbf{V}}{dt} = -\,[\,\mathbf{I} - \mathbf{V}(\mathbf{q})\mathbf{V}^T(\mathbf{q})\,]\,\mathbf{H}(\mathbf{q})\mathbf{V}(\mathbf{q}) \tag{5}$$

where, $\mathbf{V}(\mathbf{q}) = [\,\mathbf{v}_1(\mathbf{q})|\ldots|\mathbf{v}_s(\mathbf{q})\,]$ is a matrix function of $\mathbf{q}$ of dimension $(N\times s)$, such that $\mathbf{V}^T(\mathbf{q})\mathbf{V}(\mathbf{q}) = \mathbf{I}_s$, being $\mathbf{I}_s$ the unit matrix of dimension $(s\times s)$. The solution of a generalized GAD (GGAD) is a curve, $\mathbf{q}(t) = \mathbf{q}(\mathbf{q}_0, \mathbf{v}_1^0, \ldots, \mathbf{v}_s^0, t)$, guided by the set of vectors collected in the $\mathbf{V}(\mathbf{q})$ matrix, $\mathbf{v}_i(t) = \mathbf{v}_i(\mathbf{q}_0, \mathbf{v}_1^0, \ldots, \mathbf{v}_s^0, t)$ for $i = 1, \ldots, s$, which are solution of Eqs. (4) and (5) respectively. In the expressions, $\mathbf{q}(t_0) = \mathbf{q}_0$ and $\mathbf{v}_i(t_0) = \mathbf{v}_i^0$ for $i = 1, \ldots, s$. Note that in the first GAD paper [43] there is already another proposal for a GGAD method. The GGAD for a curvilinear metric different to the unit metric is proposed and discussed elsewhere [47]. The general behavior of GAD and GGAD on a PES is the following: starting near a minimum it either finds the transition state or the desired saddle point of any index by a gentlest ascent, or it can go over a TP and then find the desired saddle point of any index by going 'back' in the energy. In particular, when we are interested in the location of a TS, the case $s = 1$, then a TP occurs at the point of the curve such that the gradient and the $\mathbf{v}$-vector form an angle of $\pi/4$ radians.

Normally, GAD goes downhill after a turning point along a ridge until the transition state is located. Note: GAD can show a 'chaotic' evolution, like on the Müller-Brown PES [52] as it is described elsewhere [46]. The 'chaotic' behavior is characterized by the fact that the GAD curve goes on and back, from one TP to the next, and again back, and finally, it can end this behavior locating a TS. For the location of a stationary point of index s, if the sum of the square of the components of the projected gradient vector in the subspace spanned by the set of $\{\mathbf{v}_1, \ldots, \mathbf{v}_s\}$-vectors is higher than $1/2$, then the GGAD curve evolves in the direction of an increasing potential energy. If it is lower than $1/2$ then it evolves in the direction of a decrease of the potential energy. When the sum is equal to $1/2$ then the GGAD curve is at a turning point.

The extension of GAD and GGAD to a kind of molecular dynamics was proposed by Samanta and E [49]. The dynamics is labeled as MD-GGAD or, if $s = 1$, by MD-GAD. The dynamical equations are

$$\begin{aligned}
\frac{d\mathbf{q}}{dt} &= \mathbf{p} \\
\frac{d\mathbf{p}}{dt} &= -\,[\,\mathbf{I} - 2\mathbf{V}(\mathbf{q})\mathbf{V}^T(\mathbf{q})\,]\,\mathbf{g}(\mathbf{q}) \\
\frac{d\mathbf{V}}{dt} &= -\,[\,\mathbf{I} - \mathbf{V}(\mathbf{q})\mathbf{V}^T(\mathbf{q})\,]\,\mathbf{H}(\mathbf{q})\mathbf{V}(\mathbf{q})
\end{aligned} \tag{6}$$

where as before, $\mathbf{V}^T\mathbf{V} = \mathbf{I}_s$, with the initial conditions, $\mathbf{q}(t_0) = \mathbf{q}_0$, a point near a minimum, $\mathbf{p}(t_0) = \mathbf{p}_0 = \mathbf{0}$ and $\mathbf{V}(t_0) = \mathbf{V}_0$. The set of vectors that build the $\mathbf{V}_0$

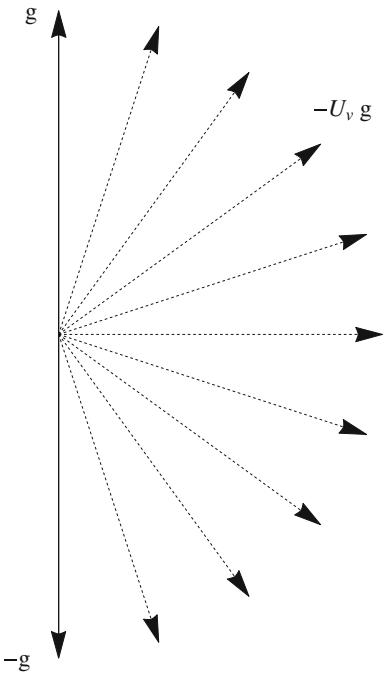

Scheme 2 Gradient vector and transformed vectors $-\mathbf{U_v g}$ which are from the pathway of an MD-GAD curve, are superimposed in one point. To get a full cancelation of the gradient parts (the vertical ones), the curve has to go up to a TP of MD-GAD. There is $-\mathbf{U_v g} = -\mathbf{g}$

matrix can be preferably either a selected subset of the eigenvectors of the Hessian matrix evaluated at the point $\mathbf{q}_0$, or it can be some subset of the columns of the unit matrix or any other set of vectors: see the next Section for some tests on this matter. The dimension of system (6) is $(2 + s) \times N$.

Note that the MD-GGAD curves solving system (6) are others in comparison to the trajectories of the pure GGAD system, Eqs. (4) and (5). The solution of both systems can pass a TS – that is the property for which both where defined. However, already the 'passing' of the TS may be different: At the TS, and if the vectors of $\mathbf{V}$ are turned to eigenvectors orthogonal to $\mathbf{g}$ only, the second and the third part of system (6) are zero vectors. Thus, the help vector $\mathbf{p}$ does not change there, it will be a constant vector. The curve $\mathbf{q}(t)$ will be a straight piece through the TS and it will continue at the 'other side' of the TS. In contrast, a solution of Eqs. (4) and (5) can circumnavigate the TS in many 'infinitely small' steps [47].

Still more complicated is the emergence of TPs on a MD-GAD trajectory. At a TP the tangent to the MD-GAD curve has to point orthogonally to the gradient. The vector $d\mathbf{q}/dt = \mathbf{p}$ has to lie again in the tangential hyperplane of the equipotential hypersurface of the PES. However, $\mathbf{p}$ is updated before, if we integrate it along the full MD-GAD trajectory. It may be started near the minimum of the PES with $\mathbf{p} = \mathbf{0}$. There is $-\mathbf{U_v g} = \mathbf{g}$, but the vector $-\mathbf{U_v g}$ may turn along the MD-GAD curve. To reach a vector $\mathbf{p} \perp \mathbf{g}$ all the 'vertical' parts of the initial gradient have to be canceled out: this can happen if the turning of $-\mathbf{U_v g}$ takes place up to $-\mathbf{U_v g} = -\mathbf{g}$, compare Scheme 2. But then $\mathbf{v}$ itself is orthogonal to $\mathbf{g}$. We observe this property below in all examples of MD-GAD trajectories with TPs.

A direct development of the TP property is the following reasoning: If an MD-GAD trajectory has a TP on the PES then we have the condition at the TP, namely, $dW(\mathbf{q})/dt = 0$. We can write:

(i) $dW(\mathbf{q})/dt = \mathbf{g}^T\ \mathbf{p} = 0$, where the first expression of Eq. (6) is used. Second, if the trajectory has a TP, then, with the condition (i), $\mathbf{p}$ itself turns. Thus $|\mathbf{p}|$ has a maximal length and it holds
(ii) $\frac{1}{2}d(\mathbf{p}^T\mathbf{p})/dt = 0 = (d\mathbf{p}/dt)^T\mathbf{p} = \mathbf{f}^T\ \mathbf{p}$, where Eq. (1) and the second expression of Eq. (6) are used.

Following the second condition and using the definition of $\mathbf{f}$ we have that

$$0 = \mathbf{p}^T\ \mathbf{g}\ - 2\mathbf{p}^T\ \mathbf{v}\ \mathbf{v}^T\ \mathbf{g} = -2\mathbf{p}^T\ \mathbf{v}\ \mathbf{v}^T\ \mathbf{g},$$

due to condition (i). We assume without a loss of generality the norm $\mathbf{v}^T\mathbf{v} = 1$. The second condition is zero if (a) $\mathbf{v}$ is orthogonal to $\mathbf{g}$ or (b) $\mathbf{p}$ is orthogonal to $\mathbf{v}$ implying that $\mathbf{v}$ is parallel to $\mathbf{g}$. The conditions (i) and (ii, a) act for a TP whereas the conditions (i) and (ii, b) do not fit at a TP by construction: if $\mathbf{v}$ is parallel to $\mathbf{g}$, then it is $-\mathbf{U}_\mathbf{v}\mathbf{g} = \mathbf{g}$ which means that $\mathbf{p}(t)$ would go uphill along the steepest ascent.

The Eq. (6) can be justified by defining, firstly, the integral function,

$$I(\mathbf{q}) = \int_{t_0}^{t} L\left(\frac{d\mathbf{q}}{dt'}, \mathbf{q}\right) dt' = \int_{t_0}^{t} \left[\frac{1}{2}\left(\frac{d\mathbf{q}}{dt'}\right)^T \left(\frac{d\mathbf{q}}{dt'}\right) - \Theta(\mathbf{q})\right] dt' \tag{7}$$

where the image potential function, $\Theta(\mathbf{q})$, depends parametrically on the set of guide vectors, $\{\mathbf{v}_1, \ldots, \mathbf{v}_s\}$, and secondly, applying the Legendre transformation [50] to the functional L of Eq. (7) which results in the corresponding Hamiltonian expression. From this Hamiltonian expression and Eq. (1) the first two expressions of Eq. (6) are obtained being the actual Hamiltonian equations of the present problem.

However, as shown elsewhere [46], the Jacobian is non-symmetric, in general

$$\left(\nabla_\mathbf{q}\mathbf{f}^T(\mathbf{q})\right)_{ij} \neq \left(\nabla_\mathbf{q}\mathbf{f}^T(\mathbf{q})\right)_{ji}$$

for $i \neq j$ implying that

$$\Theta(\mathbf{q}_1) - \Theta(\mathbf{q}_0) \neq \int_{t_0}^{t_1} \mathbf{f}^T(\mathbf{q}) \left(\frac{d\mathbf{q}}{dt}\right) dt = \int_{t_0}^{t_1} \mathbf{f}^T(\mathbf{q})\mathbf{p}dt \tag{8}$$

where the first expression of Eq. (6) is used. Due to this result, the image gradient field vector should be considered as a nonconservative force field. From this fact follows that a unique image of the PES function does, in general, not exis [45,46], and the previous arguments to justify the first two expressions of Eq. (6) are only true if a quadratic expansion around $\mathbf{q}$ is considered. These results show that the MD-GGAD is not conservative. For the same reasons the third part of Eqs. (6) is needed to select a member of the family of the image PES functions during the evolution.

Finally, E et al. [43,49] studied the stability of GAD and MD-GAD models concluding that for minimums of the PES both are unstable, however, both are stable for transition states.

3 Behavior in two-dimensional potential surfaces

The set of Eq. (6) that characterizes the MD-GGAD model has been integrated using the explicit Runge-Kutta method of order 8(5,3) [53]. We have used two-dimensional PES models to analyze the behavior of the MD-GAD trajectories for $s = 1$. We understand by an MD-GAD trajectory the projection of the MD-GAD curve in the configuration space of (x,y).

3.1 Wolfe–Quapp model

The first PES model used for this purpose is the Wolfe-Quapp PES [54,55]. The equation of this surface model is

$$W(x, y) = x^4 + y^4 - 2x^2 - 4y^2 + xy + 0.3x + 0.1y \tag{9}$$

which is depicted in Fig. 1. We look for three MD-GAD trajectories all starting near the minimum MIN3 located at the point $(1.124, -1.485)$ with energy in arbitrary units -6.37. The first MD-GAD curve starts at the point $(x, y, p_x, p_y, v_x, v_y) = (1.1, -1.4, 0, 0, 0.189, 0.982)$ where the initial **v**-vector is an eigenvector of the Hessian matrix at the initial point. The trajectory reaches the transition state located at $(0.941, 0.131)$ and labeled as TS3 with energy -0.64. From this point the trajectory crosses the valley where the minimum MIN1 is located and at the point $(0.496, 1.905)$ it turns back, it crosses the valley again, and at the end it points in the direction of the MAX stationary point located at $(0.081, 0.023)$ with energy 0.013. From this behavior follows that the point $(0.496, 1.905)$ is a turning point (TP) of this MD-GAD trajectory. The amplified part of the PES around the TP is seen in Fig. 2. The arrows in magenta are the gradient vectors, the green arrows are the **v**-vectors and the black arrows are the momentum, that according to the first Eq. (6) are also the tangent vectors. At the TP the **v**-vector and the momentum point in the same direction while the gradient vector is orthogonal to this direction. Thus a TP occurs on the MD-GAD trajectory if $\mathbf{g}^T(\mathbf{q})\mathbf{p} = 0$ implying that $dW(\mathbf{q})/dt = \nabla_{\mathbf{q}}^T W(\mathbf{q}) d\mathbf{q}/dt = \mathbf{g}^T(\mathbf{q}) d\mathbf{q}/dt = \mathbf{g}^T(\mathbf{q})\mathbf{p} = 0$, where the first expression of Eq. (6) and the concept of the direction derivative have been used. In addition to this condition we have $\mathbf{p} = \alpha\mathbf{v}$, being α a proportionality factor because $\mathbf{v} \perp \mathbf{g}$ as well. According to the condition at the TP the **p** vector has to point along the level line. The second condition is due to the structure of the GAD model. With these considerations the two first expressions of Eq. (6) reduce to the standard Hamiltonian equations.

The piece of the trajectory from the starting point near to the minimum, MIN3, up to the TP is located in a valley region of the PES. A valley is defined as the part of the PES where $\mathbf{g}^T\mathbf{A}\mathbf{g} > 0$ being **A** the adjoint matrix of the Hessian matrix, **H**, while a region where each point satisfies $\mathbf{g}^T\mathbf{A}\mathbf{g} < 0$ is a ridge region [56]. The line that

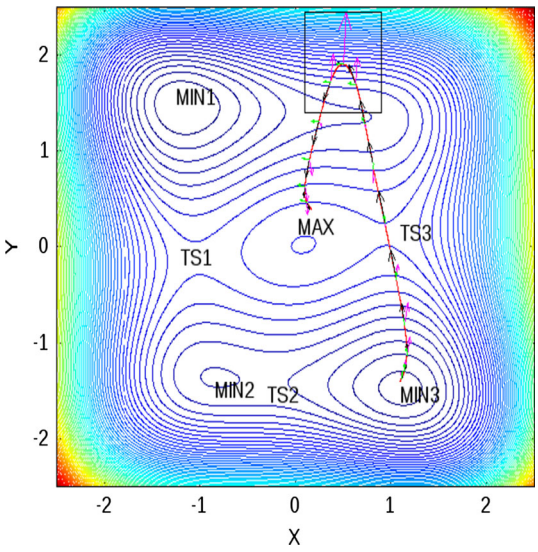

Fig. 1 An MD-GAD trajectory in *orange color*, on the Wolfe–Quapp PES, Eq. (9). The trajectory starts at the point $(x, y, p_x, p_y, v_x, v_y) = (1.1, -1.4, 0, 0, 0.189, 0.982)$. The initial guide vector is the eigenvector of the first eigenvalue of the Hessian matrix evaluated at the starting point. *Color key*: The *black arrows* are the tangent vectors of the trajectory, $d\mathbf{p}/dt$, the *green arrows* are the guide $\mathbf{v}$-vectors with their evolution along the trajectory while the *arrows* in *magenta* are the gradient vectors of the PES. The region marked by a *black square* is where a TP of the trajectory occurs. This region is amplified in Fig. 2 (Color figure online)

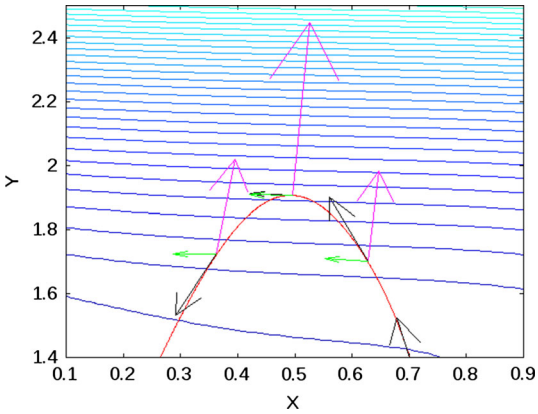

Fig. 2 The amplified region of the PES indicated in Fig. 1. *Color key*: The trajectory is depicted in *red*. The gradient vectors are depicted in *magenta*, while the tangent vectors and the guide vectors have *black* and *green colors* respectively. Note that at the TP, the relations $\mathbf{g}^T(\mathbf{q})\mathbf{p} = 0$ and $\mathbf{p} = \alpha\mathbf{v}_1$, are satisfied (Color figure online)

separates both regions satisfies the relation $\mathbf{g}^T\mathbf{A}\mathbf{g} = 0$ and it is known as the valley-ridge transition line, and the special point of this line with the property $\mathbf{A}\mathbf{g} = \mathbf{0}$ is a valley-ridge inflection point [57,58]. Because from the starting point up to the TP the GAD trajectory is located in a valley where any reaction path joining the minimums MIN1 and MIN3 through TS3 is also located, we can say that this sub-arc of the MD-GAD trajectory well represents a reaction path dynamical trajectory.

When the trajectory of Fig. 1 comes near the MAX point then it turns again and finds the TS3. After this it starts a 'coming return' behavior in the region where the transition states, TS1 and TS3, are located, see Fig. 3. Like the GAD curve [46], the MD-GAD also shows a kind of 'chaotic' behavior going on and back, from one TP to the next. The permanence of the trajectory in this region can be justified by the stability analysis of the MD-GAD reported in reference [49]. Note that the TS1 and TS3 are crossed, nevertheless.

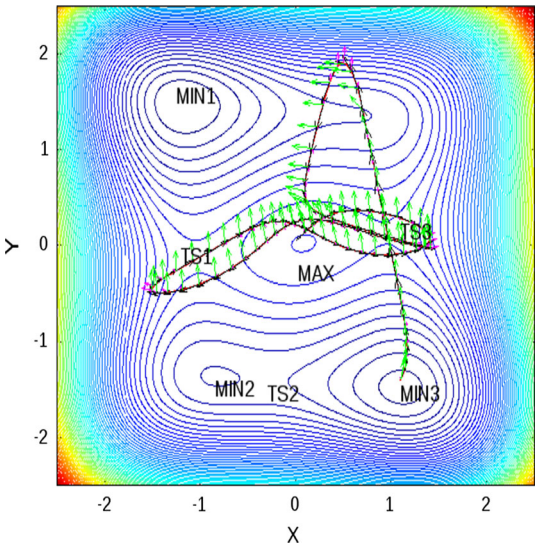

Fig. 3 The trajectory of Fig. 1 elongated for the parameter t after the second TP. It enters a region where the stationary points, TS1, TS3 and MAX, are located. In this region the trajectory shows a 'chaotic' behavior going on and back, from one turning point to the next, and again back. *Color key*: the *green arrows* are the guide vectors, the *magenta arrows* are the gradient vectors of the PES while the *black arrows* are the tangent vectors of the trajectory (Color figure online)

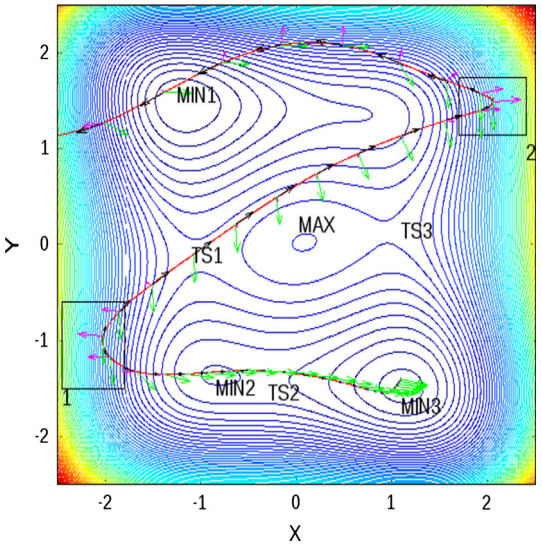

Fig. 4 An MD-GAD trajectory in *red color*, starting at the point $(x, y, p_x, p_y, v_x, v_y) = (1.1, -1.4, 0, 0, 0.982, -0.189)$. The initial guide vector is the eigenvector of the second eigenvalue of the Hessian matrix evaluated at the starting point. The *black arrows* are the momentum or tangent vectors of the trajectory, the *green arrows* are the guide **v**-vectors while the *arrows* in *magenta* are the gradient vectors of the PES. The regions marked by a *black square* are where a TP of the trajectory occurs. The comparison of the trajectory with that depicted in Fig. 1 is that this one is very different. However both differ only in the initial guide **v**-vector. The trajectory here does not show any 'chaotic' behavior (Color figure online)

A similar behavior is found when an MD-GAD curve starts near the minimum MIN3 but with a different guide **v**-vector, see Fig. 4. More specifically, the initial point of the curve now is $(x, y, p_x, p_y, v_x, v_y) = (1.1, -1.4, 0, 0, 0.982, -0.189)$

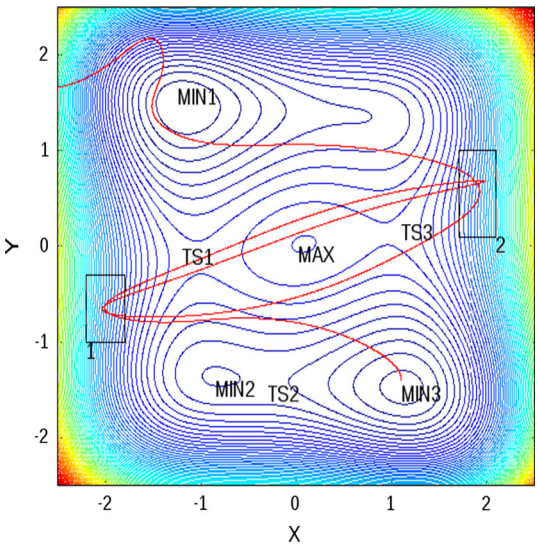

Fig. 5 MD-GAD trajectory, depicted in *red color*, but starting at the point $(x, y, p_x, p_y, v_x, v_y) = (1.1, -1.4, 0, 0, 0, 1)$. The initial guide vector is the second column of the unit matrix. The regions marked by a *black square* contain a TP of the trajectory. The trajectory also shows 'less chaotic' behavior in the region where TS1, TS3 and MAX stationary points are located (Color figure online)

and the corresponding trajectory reaches the TS2 and touches the MIN2 located at $(-0.30, -1.4)$ and $(-0.82, -1.37)$ with energies -3.98 and -4.14, respectively. The trajectory leaves the valley where the minimum MIN2 is located and passes a TP located at $(-2.03, -1)$ being the center of the square labeled by **1** in Fig. 4. We emphasize that from MIN3 to MIN2 the trajectory behaves as a reaction path dynamical trajectory, but around the TP it leaves the valley and starts to descend along a ridge, and after this it passes through the transition state TS1 located at $(-1.02, -0.12)$, with energy -1.25. The trajectory continues until its second TP located at $(2.06, 1.49)$, where it turns back into the valley where the minimum MIN1 is located. The trajectory passes nearby. Note that meeting exactly the minima is not the task of our kind of trajectories, as well as it is not the task to meet SPs of index two, the MAX point here, for $s = 1$. The second TP is labeled by **2** in Fig. 4. Finally, the trajectory leaves the region of Fig. 4. A similar behavior is found for the same PES using the pure GAD model [46].

Now, we study the effect of the evolution of the MD-GAD curve due to a next modification of the initial **v**-vector. We start at the same point and zero momentum but the initial guide vector is the second column of the unit matrix, $(x, y, p_x, p_y, v_x, v_y) = (1.1, -1.4, 0, 0, 0, 1)$. The resulting trajectory is shown in Fig. 5. It is different with respect to the two previous ones. The trajectory in general does not follow a valley. It omits TS2 and MIN2 and it reaches immediately a TP in the region marked by **1** in Fig. 5 and it goes then to the second TP in the region denoted by **2**, passing through the TS1 and touching near the MAX point. It again goes back to the region **1** and after the TP it goes again to the region **2**. However, after the TP it can leave the region and it enters into the region of the valley where MIN1 is located. Finally it leaves the area of Fig. 5.

From the three results we conclude that the initial guide vectors strongly effect the general behavior of the MD-GAD trajectory. But all the example trajectories behave

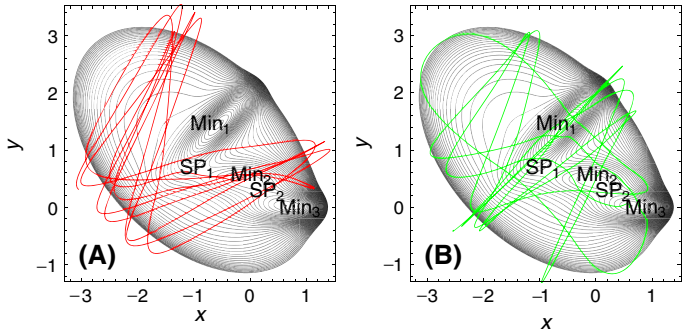

Fig. 6 The behavior of the MD-GAD trajectories in the Müller–Brown PES model [52]. **a** The *red* trajectory starts near the minimum MIN_2 whereas **b** the *green* trajectory starts near the minimum MIN_3 (Color figure online)

as expected: they meet TSs, they touch minima or SPs of index two. And in all the TPs we have found that the relations $\mathbf{g}^T\mathbf{p} = 0$ and $\mathbf{p} = \alpha\mathbf{v}$ are satisfied.

3.2 Müller–Brown model

One of the most widely used two-dimensional surface for a test model is the Müller-Brown PES [52]. This PES can be associated to a reaction mechanism of the form $R \rightleftharpoons I \rightharpoonup P$ where the reactant, R, is the minimum MIN_3, the intermediate, I, is the minimum MIN_2 and the product, P, is the minimum MIN_1. Between MIN_3 and MIN_2 the transition state, TS_2, is located and between MIN_2 and MIN_1 the transition state, TS_1, is located. Figure 6 shows the behavior of two MD-GAD trajectories where the level lines (in black color) are only drawn up to 222 arbitrary energy units.

The red trajectory starts near the minimum, MIN_2, with an initial point of its MD-GAD curve $(x, y, p_x, p_y, v_x, v_y) = (-0.1, 0.45, 0, 0, 0.122, 0.922)$. The green trajectory starts near the minimum, MIN_3, and the initial point of its MD-GAD curve is $(x, y, p_x, p_y, v_x, v_y) = (0.6, 0, 0, 0, 0.24, 0.999)$. Both trajectories show a 'chaotic' behavior, however, whereas the red one spends a part of its evolution in the region where the stationary points TS_1, TS_2 and MIN_2 are located, the green one develops into the deep valley of the stationary point MIN_1. This behavior of the MD-GAD trajectories is close to that shown by the pure GAD curve on the same surface [46].

3.3 Ackley model

This surface model is characterized by the equation [59]

$$W(x, y) = -20 \exp\left(-0.2\sqrt{\frac{x^2 + y^2}{2}}\right) - \exp\left(\frac{\cos(2\pi x) + \cos(2\pi y)}{2}\right) + 20 + \exp(1) \tag{10}$$

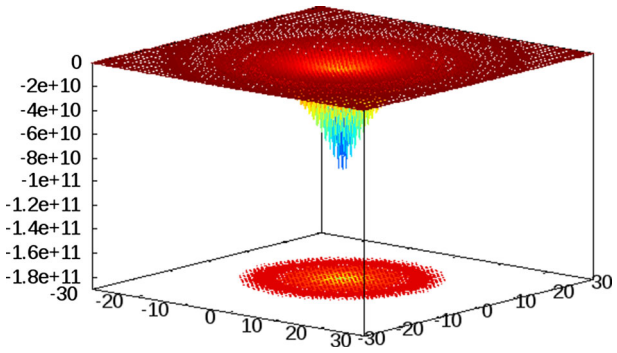

Fig. 7 The Ackley surface given in Eq. (10). Its projection in the x, y-plane is also shown. The features of the PES of a protein folding as described elsewhere [60] are well represented by this PES model. The deep minimum located in the (0, 0) point is associated to the native conformation of the protein

The surface is characterized by a nearly flat outer region, and by a large hole in the center. It is the global minimum at the point (0, 0). There holds $W(0, 0) = 0$ and the gradient vector becomes singular, as well as all the elements of the Hessian are indeterminate. This implies that the Ackley surface, Eq. (10), is a continuous function but it is not derivable in the center point [47]. In Fig. 7 we show the Ackley surface.

The Ackley surface has a useful chemical region in the square domain, $[-40, 40] \times [-40, 40]$. Its topography is close to that proposed as the PES model of a protein folding rearrangement [60]. In the model, the native conformation of the protein is located in the global minimum, (0, 0), and the minimums around the deep valley are related to the conformations associated to the denatured states of the protein. These minimums have direct access to the native conformation. The far minimums with respect to the global minimum are related to the dead-end denatured conformations. To reach the global minimum related to the native conformation, any conformation beginning in the dead-end region of the PES must first pass through the conformations of denatured states that are located around the deep native valley. The features of the PES of a protein folding [60] are well represented by the model of the Ackley surface given in Eq. (10).

In Fig. 8 we show the behavior of two MD-GAD trajectories starting near the global minimum but with different initial **v**-vectors. The MD-GAD curve that results in the black trajectory starts at the point $(x, y, p_x, p_y, v_x, v_y) = (0, 0.001, 0, 0, 1, 0)$ while the blue trajectory is the MD-GAD curve that starts at the point $(x, y, p_x, p_y, v_x, v_y) = (0.005, 0.001, 0, 0, -0.195, 0.981)$. Both trajectories start near the deep global minimum. The main difference is the initial **v**-vector. The guide **v**-vector of the black trajectory is the first vector of the unit matrix and the trajectory evolves in the lower right hand side part of the surface. The guide **v**-vector of the blue trajectory is the eigenvector of the lowest eigenvalue of the Hessian matrix computed in the initial point. In this case the trajectory goes in the direction of the x-axis. As opposed to the previous PES models, here no trajectory has a TP.

Figure 9 shows an enlarged piece of one of the MD-GAD trajectories of the last Fig. 8. The region $x \in [17, 20]$, $y \in [-17, -20]$ is given to show the exact trajectory through the TS at $(18.5, -19)$.

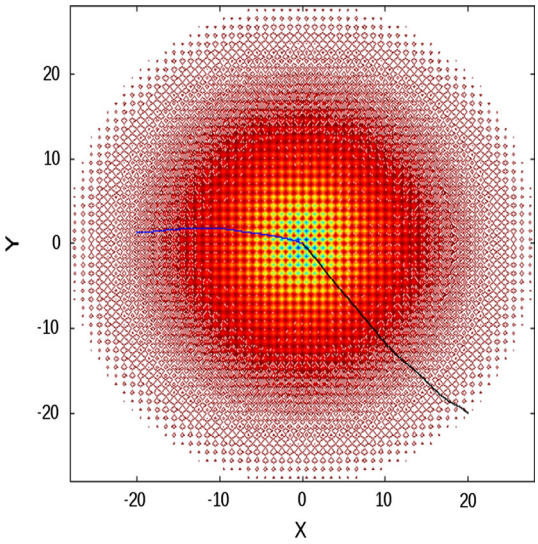

Fig. 8 The behavior of two MD-GAD trajectories in the Ackley surface. Both trajectories start near the deep minimum located in (0, 0). The *black* trajectory results from the MD-GAD curve that starts at the point $(x, y, p_x, p_y, v_x, v_y) = (0, 0.001, 0, 0, 1, 0)$ while the *blue* one starts at the point $(x, y, p_x, p_y, v_x, v_y) = (0.005, 0.001, 0, 0, -0.195, 0.981)$. None of both trajectories show TPs (Color figure online)

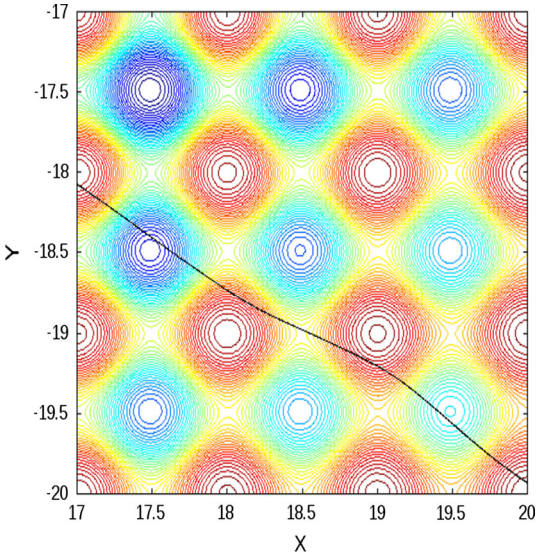

Fig. 9 Enlarged piece of the right MD-GAD trajectory of the last figure

4 Conclusions

We have analyzed the evolution of MD-GAD trajectories in two-dimensional PESs, as a model of a general potential surface associated to a chemical reaction. An MD-GAD trajectory shows a similar evolution and behavior with respect to the older GAD pathway. The MD-GAD trajectory can cross a region of the PES where a transition state exists. This was the reason for defining it. Then it can hop to a next TS touching

a minimum or an SP of index two in between. The MD-GAD trajectory is usually stable at TSs as proved through the analysis of Samanta and E [49].

Different initial guide vectors for the same initial position and zero momentum give qualitatively different trajectories. We conclude form the analysis that either GAD or MD-GAD can be used to locate transition states starting from a minimum in an automatic and autonomous way if a corresponding guide vector is used.

However, also MD-GAD trajectories can go, like GAD pathways [46], over turning points (TP). They can start there a quasi-periodic, or 'chaotic' dynamics. Every TP is characterized by the relations $\mathbf{g} \perp \mathbf{p}$ and $\mathbf{v}||\mathbf{p}$. Trajectories crossing a TP are only initially located in a reaction valley, but regions containing the TP are usually ridges of the PES. Such trajectories cannot be taken as a general reaction path dynamical trajectory.

Finally, a major drawback of the MA-GAD method is that it will be time-consuming for complex molecular systems due to the Hessian matrix evaluation.

Acknowledgments Financial support has been provided by the Spanish Ministerio de Economía y Competitividad (formaly Ministerio de Ciencia e Innovación) through Grant No. CTQ2011-22505 and by the Generalitat de Catalunya through Grant No. 2009SGR-1472, and XRQTC.

References

1. P.G. Mezey, *Potential Energy Hypersurfaces* (Elsevier, Amsterdam, 1987)
2. D. Heidrich (ed.), *The Reaction Path in Chemistry: Current Approaches and Perspectives* (Kluwer, Dordrecht, 1995)
3. W.H. Miller, N.C. Handy, J.E. Adams, J. Chem. Phys. **72**, 99 (1980)
4. J. González, X. Giménez, J.M. Bofill, J. Phys. Chem. A **105**, 5022 (2001)
5. J. González, X. Giménez, J.M. Bofill, J. Comput. Chem. **28**, 2111 (2007)
6. J. González, X. Giménez, J.M. Bofill, J. Chem. Phys. **131**, 054108 (2009)
7. D.G. Truhlar, B.C. Garret, Annu. Rev. Phys. Chem. **35**, 159 (1984)
8. J. González, X. Giménez, J.M. Bofill, Phys. Chem. Chem. Phys. **4**, 2921 (2002)
9. P. Hänggi, P. Talkner, M. Borkovec, Rev. Mod. Phys. **62**, 251 (1990)
10. W. Quapp, D. Heidrich, Theor. Chim. Acta **66**, 245 (1984)
11. K. Fukui, J. Phys. Chem. **74**, 4161 (1970)
12. M.J. Rothman, L.L. Jr Lohr, Chem. Phys. Lett. **70**, 405 (1980)
13. P. Scharfenberg, Chem. Phys. Lett. **79**, 115 (1981)
14. I.H. Williams, J. Mol. Struct. THEOCHEM **89**, 365 (1982)
15. W. Quapp, M. Hirsch, O. Imig, D. Heidrich, J. Comput. Chem. **19**, 1087 (1998)
16. J.M. Anglada, E. Besalú, J.M. Bofill, R. Crehuet, J. Comput. Chem. **22**, 387 (2001)
17. W. Quapp, M. Hirsch, D. Heidrich, Theor. Chem. Acc. **100**, 285 (1998)
18. J.M. Bofill, W. Quapp, J. Chem. Phys. **134**, 074101 (2011)
19. D.K. Hoffman, R.S. Nord, K. Ruedenberg, Theor. Chim. Acta **69**, 265 (1986)
20. W. Quapp, Theor. Chim. Acta **75**, 447 (1989)
21. M.V. Basilevsky, Chem. Phys. **67**, 337 (1982)
22. J.-Q. Sun, K. Ruedenberg, J. Chem. Phys. **98**, 9707 (1993)
23. K. Bondensgård, F. Jensen, J. Chem. Phys. **104**, 8025 (1996)
24. J.M. Bofill, W. Quapp, M. Caballero, J. Chem. Theory. Comput. **8**, 927 (2012)
25. H.B. Schlegel, in *Modern Electronic Structure Theory*, ed. by D.R. Yarkony (World Scientific Publishing, Singapore, 1995), p. 459
26. R. Crehuet, J.M. Bofill, J. Chem. Phys. **122**, 234105 (2005)
27. A. Aguilar-Mogas, R. Crehuet, X. Giménez, J.M. Bofill, Mol. Phys. **105**, 2475 (2007)
28. W. Quapp, Theor. Chem. Account. **121**, 227 (2008)
29. G.M. Crippen, H.A. Scheraga, Arch. Biochem. Biophys. **144**, 462 (1971)

30. R. Fletcher, *Practical Methods of Optimization* (Wiley, New York, 1987)
31. S. Bell, J.S. Crighton, J. Chem. Phys. **80**, 2464 (1984)
32. A. Banerjee, N. Adams, J. Simons, R. Shepard, J. Phys. Chem. **89**, 52 (1985)
33. J. Baker, J. Comput. Chem. **7**, 385 (1986)
34. T. Helgaker, Chem. Phys. Lett. **182**, 503 (1991)
35. P. Culot, G. Dive, V.H. Nguyen, J.M. Ghuysen, Theor. Chim. Acta **82**, 189 (1992)
36. J.M. Bofill, J. Comput. Chem. **15**, 1 (1994)
37. P.Y. Ayala, H.B. Schlegel, J. Chem. Phys. **107**, 375 (1997)
38. E. Besalú, J.M. Bofill, Theor. Chem. Acc. **100**, 265 (1998)
39. L.J. Munro, D.J. Wales, Phys. Rev. B **59**, 3969 (1999)
40. G. Henkelman, H. Jónsson, J. Chem. Phys. **111**, 7010 (1999)
41. A. Poddey, P.E. Blöchl, J. Chem. Phys. **128**, 044107 (2008)
42. G.T. Barkema, N. Mousseau, Phys. Rev. Lett. **77**, 4358 (1996)
43. W. E, X. Zhou, Nonlinearity **24**, 1831 (2011)
44. C.M. Smith, Theor. Chim. Acta **74**, 85 (1988)
45. J.Q. Sun, K. Ruedenberg, J. Chem. Phys. **101**, 2157 (1994)
46. J.M. Bofill, W. Quapp, M. Caballero, Chem. Phys. Lett. **583**, 203 (2013)
47. W. Quapp, J.M. Bofill, Theor. Chem. Acc. **133**, 1510 (2014)
48. Y. Zeng, P. Xiao, G. Henkelman, J. Chem. Phys. **140**, 044115 (2014)
49. A. Samanta, W. E, J. Chem. Phys. **136**, 124104 (2012)
50. I.M. Gelfand, S.V. Fomin, *Calculus of Variations* (Dover Publications, New York, 2000)
51. W. E, W. Ren, E. Vanden-Eijden, J. Chem. Phys. **126**, 164103 (2007)
52. K. Müller, L.D. Brown, Theor. Chim. Acta **53**, 75 (1979)
53. E. Hairer, S.P. Nørsett, G. Wanner, *Solving Ordinary Differential Equations I: Nonstiff Problems. Springer Series in Computational Mathematics*, 2nd edn. (Springer, Heidelberg, 1993)
54. S. Wolfe, H.B. Schlegel, I.G. Csizmadia, F. Bernardi, J. Am. Chem. Soc. **97**, 2020 (1975)
55. W. Quapp, J. Chem. Phys. **122**, 174106 (2005)
56. M. Hirsch, W. Quapp, J. Math. Chem. **36**, 307 (2004)
57. W. Quapp, M. Hirsch, D. Heidrich, Theor. Chem. Acc. **112**, 40 (2004)
58. J.M. Bofill, W. Quapp, J. Math. Chem. **51**, 1099 (2013)
59. A.R. Hedar, Global Optimization Test Problems. Technical report (2013) see also http://www.optima.amp.i.kyoto-u.ac.jp/member/student/hedar/Hedar_files/TestGO.htm
60. K. Ghosh, S.B. Ozkan, K.A. Dill, J. Am. Chem. Soc. **129**, 11920 (2007)